HHS Public Access

Author manuscript

Nanoscale. Author manuscript; available in PMC 2018 April 13.

Published in final edited form as:

Nanoscale. 2017 April 13; 9(15): 4928–4933. doi:10.1039/c7nr00888k.

pH-responsive Fluorescent Graphene Quantum Dots for Fluorescence-Guided Cancer Surgery and Diagnosis

Zetan Fan[a], **Shixin Zhou**[b], **Cesar Garcia**[c], **Louzhen Fan**[a], and **Jiangbing Zhou**[c]

[a]Department of Chemistry, Beijing Normal University, Beijing, 100875, China

[b]Department of Cell Biology, School of Basic Medicine, Peking University Health Science Center, Beijing, 100191, China

[c]Department of Neurosurgery, Yale University, New Haven, CT, 06510, USA

Abstract

Cancer remains a major cause of morbidity and mortality around the world. Improved cancer treatment requires enhancing cancer diagnosis and detection. To achieve this goal, here we reported a novel imaging probe, pH-responsive fluorescent graphene quantum dots (pRF-GQDs). pRF-GQDs were prepared by electrolysis of graphite rods in sodium p-toluenesulfonate acetonitrile solution. The resulting pRF-GQDs, which have minimal toxicity, display a sharp fluorescence transition between green and blue at pH 6.8, a pH matching the acidic extracellular microenvironment in solid tumors. We found that this unique fluorescence switch property allows distinguishing tumors from normal tissues. In addition to fluorescence, pRF-GQDs also bear the upconversion photoluminescence (UCPL) property. We demonstrate that the combination of UCPL and fluorescence switch enables detecting solid tumors of different origin at an early developmental stage. Therefore, pRF-GQDs have great potential to be used as a universal probe for fluorescence-guided cancer surgery and cancer diagnosis.

Introduction

Cancer is the leading cause of mortality worldwide. Prognosis for many cancers, such as triple negative breast cancer, pancreatic cancer, and glioblastomas, remains dismal. Promising approaches to significantly improving the survival of cancer patients include detecting tumors at an early stage before they have the chance to grow larger or metastasize as well as by improving tumor resection through identification of cancerous tissues.[1–3] In the current standard care, cancer diagnosis relies on detecting classic cancer molecular biomarkers in combination with histopathological examination in tissue biopsies. Unfortunately, cancers of different origin often have vastly different genotypes and phenotypes.[4,5] Consequently, it is challenging to establish a universal strategy for cancer detection using conventional probes that recognize cancer-associated biomarkers.[6–8]

Correspondence to: Louzhen Fan; Jiangbing Zhou.

Electronic Supplementary Information (ESI) available: [details of any supplementary information available should be included here]. See DOI: 10.1039/x0xx00000x

Universal cancer detection can be potentially achieved by using pH-responsive probes. One of the hallmarks of solid tumor microenvironment is acidosis, which is mainly caused by lactic acid accumulation in rapidly growing tumor cells owing to their elevated rates of glucose uptake but reduced rates of oxidative phosphorylation, termed Warbur's effect.[9] Insufficient blood supply and poor lymphatic drainage, which result in hypoxia in tumors, also contribute to acidic pH in the tumor microenvironment.[10–12] The interstitial pH in typical solid tumors decreases with increasing distance from the blood vessel wall and can be as low as 5.9. The average pHs in solid tumors at normoglycemia and hyperglycemia are 6.8 and 6.4, respectively.[13] By contrast, the pH value in normal tissues is usually between 7.0 and 7.4.[11,12] As acidosis exists in solid tumors regardless of their origin, probes which respond to pH of around 6.8 could be ideal for tumor detection. pH-responsive fluorescent probes for tumor detection have been previously explored. Most existing probes are designed to exhibit low or limited fluorescence intensity in normal tissues but get activated to emit greater intensity in tumors.[14–16] Probes with two distinct, switchable fluorescences at pH 6.8 have not been documented.

Graphene quantum dots (GQDs) have been previously studied for fluorescence imaging. Compared to traditional imaging materials, including organic dyes, fluorescent proteins, and semiconductor nanocrystals, GQDs have advantages of stable photoluminescence, low cytotoxicity, excellent biocompatibility, and resistance to photobleaching.[17–23] GQDs have shown to be safe for both *in vitro* and *in vivo* use.[24–33] We recently showed that GQDs did not affect stem cells viability, proliferation, metabolism and differentiation.[34,35] GQDs have been previously engineered to respond to pH change by us and others.[36,37] Unfortunately, most of these GQDs are responsive to only highly acidic or alkaline conditions at a slow rate and thus not suitable for bioimaging.

Here, we report novel pH-responsive fluorescent GQDs, designated as pRF-GQDs, for robust and universal tumor detection (Fig. 1a). pRF-GQDs switch fluorescence from blue in physiological pH to green in acidic pH. The switch point is 6.8, which matches the pH in the extracellular microenvironment in solid tumors. In addition to fluorescence property, pRF-GQDs also emit upconversion photoluminescence (UCPL). The unique bi-phase fluorescence transition in combination with UCPL makes it possible to use pRF-GQDs for sensitive detection of solid tumors regardless of their origins or stages, and thus enable fluorescence-guided surgery and diagnosis (Fig. 1b).

Results and discussion

Synthesis and characterization of the fluorescence property of pRF-GQDs

pRF-GQDs were synthesized by electrolyzing graphite rods in 0.1 M sodium p-toluenesulfonate (TsONa) acetonitrile solution at a potential of +3.0 V for 2 h, following with dialysis against deionized water. The resulting pRF-GQDs emit green fluorescence in aqueous solution with pH below 6.8. Notably, the emitted fluorescence promptly switched to blue after exposure to pH above 6.8 (Fig. 2a). The fluorescence switch was reversible and the intensity of fluorescence was correlated with the degree of acidosis and alkalosis (Fig. S1). pRF-GQDs exhibited tremendous photostability. Continuous irradiation up to 24 hours did not diminish the fluorescence intensity (Fig. 2b).

We investigated the photoluminescence property of pRF-GQDs under different pHs based on UV-vis spectrum. At pH 6.7, the typical absorption peak at 270 nm could be assigned to the π–π* transition of graphitic sp^2 domains. A n–π* absorption band at ca. 310 nm was also observed (Fig. 2c). The photoluminescence spectrum identified one emission peak at 480 nm, exhibiting excitation-independent photoluminescence behavior (Fig. S2a). The brightness of this photoluminescence peak was quantified to be 15% in terms of the quantum yield (QY) at 380 nm excitation. A distinct photoluminescence feature was observed when pH increased above 6.8. Compared to the UV-*vis* absorption spectrum at pH 6.7, the spectrum at pH 6.8 remains the π–π* absorption peak at ca. 270 nm but without the n–π* absorption band (Fig. 2d). Correspondingly, the photoluminescence peak shifted from 480 nm to 440 nm with QY of 21%, which was independent of excitation (Fig. S2b). Fluorescence decay kinetics analysis revealed multi-exponential decays, with an average lifetime of 5.2 ns at pH 6.7 and 7.0 ns at pH 6.8 (Fig. S3).

We further investigated the UCPL property of pRF-GQDs under different pHs. Similar fluorescence transition from green to blue at pH 6.8 was also found. UCPL spectra of pRF-GQDs at pH 6.7 and 6.8 under an 800 nm femtosecond pulsed laser were acquired. As shown in Fig. 2e, f, when pH increased from 6.7 to 6.8, the emission peak shifted from 480 nm to 440 nm. The quadratic dependence between the laser power and photoluminescence intensity suggests that the UCPL emission is a two-photon excitation process (Fig. S4). The UCPL emission property of pRF-GQDs is critical for potential clinical use, as excitation at 800 nm allows for deep tissue penetration, minimal photodamage to tissues, and reduced tissue autofluorescence.

Characterization of the physical and chemical properties of pRF-GQDs

We characterized the physical and chemical characteristics of pRF-GQDs. Transmission electron microscopy (TEM) and atomic force microscopy (AFM) analyses revealed that pRF-GQDs are uniform in size with an average diameter of ca. 4 nm, topographic height of 1.6 nm, and lattice spacing of 0.21 nm (Fig. 3a–d), indicating that most pRF-GQDs consist of ca. 1–3 graphene layers. X-ray photoelectron spectroscopy (XPS) analysis suggested that pRF-GQDs are composed of carbon, nitrogen, sulfur and oxygen (Fig. 3e–h). The high resolution spectrum of C1s identified a main peak at 284.3 eV, which confirms the graphite structure (sp2 C-C). The peaks at 285.6, 286.2, 287.0 and 288.0 eV suggest the presence of C-S, C-N, and C-O, C=O, respectively. The high resolution spectrum of N1s revealed the presence of both pyridinic type and (399.7eV) and pyrrolic type (401.8 eV) N atoms. The high resolution spectrum of S2p indicated the presence of -C-SOx-(x=2, 3, 4). Fourier transform infrared (FTIR) spectrum further confirmed the presence of oxygen-containing groups (O-H, C-O, C=O) and C-S, C=C, C=N (Fig. 3i). Raman and X-ray diffraction (XRD) spectra suggested that pRF-GQDs contain numerous defects (Fig. S5a, b). pKa of the pRF-GQDs was also determined based on UV-*vis* absorption (Table S1). The calculated pKa average value was 6.6, which is close to the fluorescence switch point at pH 6.8. Based on these findings, we speculate that, in weak acidic environment, the protonated nitrogen acts as a H-bond donor to form an intramolecular N-H-O hydrogen, which further interacts with the adjacent sulfonic oxygen. This hydrogen bond interaction results in the observed fluorescence switch (Fig. 3j).

pRF-GQDs for in situ detection of tumors

The fluorescence switch property is intriguing as it may allow identification of mild acidic environments, which can be used in distinguishing normal tissues from tumors. To test this, we injected pRF-GQDs subcutaneously to tumors and adjacent muscles in mice bearing HeLa tumors. After 24 h, tumors along with adjacent muscles were excised, sectioned, and subjected to confocal fluorescence microscopy imaging. We found that, although having received the same excitation and within the same field, tumors and muscles emitted distinct fluorescences where tumors were green and muscles were blue (Fig. S6).

Compared to locoregional injection, intravenous administration is more clinically relevant. Hence, we tested pRF-GQDs for tumor detection in five different xenografts, including mice with tumors derived from human cervical cancer HeLa cells, liver cancer HepG2 cells, pancreatic cancer PANC-1 cells, lung cancer A549 cells, and glioma U87MG cells. Twenty-four hours after tail vein injection, tumors and adjacent muscles were collected, sliced and imaged by confocal fluorescence microscopy. Results in Fig. 4 showed that, across all the five tumor xenografts and with the same excitation, tumors and muscles emitted distinct fluorescences, with green for tumors and blue for muscles, respectively. The sharp difference in fluorescence emission makes it possible to use pRF-GQDs to distinguish tumors from normal tissue. In clinical applications, pRF-GQDs can be potentially used for fluorescence-guided surgery through intravenous or locoregional administration.

pRF-GQDs for non-invasive detection of tumors in live animals

Bearing the UCPL emission property, pRF-GQDs may have additional clinical applications for non-invasive tumor detection. To test this, we intravenously administrated pRF-GQDs to mice bearing HeLa tumors, which were then imaged using an IVIS Lumina III system at excitation/emission of 800 nm/520 nm. As shown in Fig. 5a, at 12 h post-injection, a clear fluorescence signal was observed at the tumor site, indicating pRF-GQDs emitted green fluorescence in the acidic tumor microenvironment. The specificity of pRF-GQDs to tumors peaked at 24 h post-injection, likely because that pRF-GQDs were excreted from other healthy organs but retained in tumors due to the enhanced permeability and retention (EPR) effect[38]. We euthanized mice at this time point and imaged various tissues. Results in Fig. 5b confirmed that pRF-GQDs preferentially identified tumors.

Extracellular acidosis exists in solid tumors regardless of tumor types. Therefore, pRF-GQDs have the potential to be used as a universal probe for detection of tumors of different origin. To confirm this, we evaluated pRF-GQDs in four additional tumor xenografts, which were derived from PANC-1 cells, HepG2 cells, A549 cells, and U87MG cells, respectively. As expected, significant fluorescent signals were detected in tumors in all four models at 12 h after intravenous administration of pRF-GQDs (Fig. 5c).

We determined the sensitivity of pRF-GQDs for tumor diagnosis. HeLa cell suspension containing 1×10^6 cells (0.1 mL) was injected subcutaneously to the right armpit of Balb/c nude mice. After implantation, the mice were intravenously administrated with pRF-GQDs solution at a dose of 5 mg/kg every two days and imaged at 12 h post-injection point after each administration. As shown in Fig. 5d, strong green fluorescent signals were detected at

the injection site starting from the 6th day after tumor implantation; at that time no obvious tumor lumps could be identified by eyes. The intensity of fluorescence increased with tumor growth. These results suggested that pRF-GQDs allow for tumor detection at an early development stage, which is crucial for enhanced cancer treatment.

Assessment of the toxicity of pRF-GQDs

We assessed the toxicity of pRF-GQDs on a panel of cell lines, including two derived from tumors, HeLa and MCF-7, and one derived from non-cancerous tissues, normal human gastric epithelial cells (GECs). pRF-GQDs were added to cells at serial concentrations. Twenty-four hours later, the viability of cells was determined. Results in Fig. 6a showed that pRF-GQDs did not exhibit obvious toxicity at concentrations up to 100 μg/mL. We further evaluated the cytotoxicity of pRF-GQDs in live animals. Healthy mice received intravenous injection of pRF-GQDs at 10 mg/kg every other day and euthanized at day 15. Major organs, including the brain, lung, liver, kidney, spleen and heart, were collected, sliced and subjected to H&E staining. We found that, compared to control naïve mice without treatments, pRF-GQDs-treated mice did not present noticeable toxicity in all the organs (Fig. 6b). Our results suggest that pRF-GQDs are potentially safe for clinical use.

Experimental

Preparation of pRF-GQDs

High purity graphite rods were purchased from Shanghai Carbon Co., Ltd. All solvents and reagents were purchased from Aladdin Industrial Corporation (Shanghai). The electrolysis of the graphite rod was performed on CHI 705a electrochemical workstation with current intensity in the range of 80–120 mA/cm^2. After a 2 h electrochemical reaction, the reactant was filtered using 0.22 μm filter membrane to remove the precipitated graphite oxide and graphite particles. The resulting pRF-GQDs solution was dialyzed against deionized water in a dialysis bag (3500 Da) for one day. The QY of the pRF-GQDs was determined by comparing the integrated photoluminescence intensities (excited at 400 nm) to the absorbance values (at 400 nm) using rhodamine 6G in ethanol (QY = 95%) as a reference.

Characterization of pRF-GQDs

Transmission electron microscopy (TEM) was carried out on JEOL JEM 2100. The atomic force microscope images were captured by MultiMode V SPM (VEECO). X-ray diffraction (XRD) patterns were acquired by using Cu K α radiation (XRD, PANalytical X'Pert Pr MPD). Fourier transform X-ray photoelectron spectroscopy (XPS) were determined by an ESCAlab 250Xi electro spectrometer from Thermo Scientific using 300 W Al K α radiation. The base pressure was about 3×10^{-9} mbar. The binding energies were referenced to the C1s line at 284.8 eV from adventitious carbon. The UV-*vis* absorption and the photoluminescence spectra were measured with a UV-2450 spectrometer and a Cary Eclipse fluorimeter, respectively. The Raman spectrum was determined using Laser Confocal Micro-Raman Spectroscopy (LabRAM Aramis).

In vivo and *ex vivo* imaging

Tumor-bearing Balb/c nude female mice were purchased from Beijing Vital River experimental animal technical co., LTD and maintained under standard housing conditions. Five tumor xenografts, which derived from HeLa, HepG2, PANC-1 cancer, A549 and U87MG cancer cells, respectively, were used to evaluate pRF-GQDs for tumor detection. All animal experiments were carried out in accordance with the guidelines approved by the ethics committee of Beijing Normal University. When the average tumor volume reached about 150 mm^3, the mice were intravenously injected with 50 μL of pRF-GQDs (5 mg/kg, n=3 for each tumor model). The fluorescence images were captured using an IVIS Lumina III system with ex. at 800 nm and em. at 520 nm 2, 6, 12 and 24 h post-injection. Images were analysed using Living Image Software. Twenty-four hours after injection, the mice were sacrificed and major organs, including the brain, kidney, heart, liver, lung, spleen and tumor, were isolated and imaged.

Cell culture

Cells using in this study, including HeLa cells, PANC-1 cells, A549 cells, HepG2 cells, U87MG cells, MCF-7 cells, and GECs, were cultured in the DMEM medium supplemented with 10 % fetal bovine serum (FBS), 100 units/mL of penicillin and 100 mg/mL of streptomycin. All the cells were incubated in a humidified atmosphere at 37 °C with 5% CO_2.

Cytotoxicity of pRF-GQDs

Cytotoxicity of pRF-GQDs was determined using the standard CCK8 tests that quantify the metabolic activity in cells. Briefly, cells were plated in 96-well microplates at a density of 1×10^4 cells per well. Twenty-four hours later, pRF-GQDs were added at a serial of concentrations and incubated with cells for 24 h. Then, the culture medium was replaced with fresh media. Ten μL of CCK8 solution was added to each well and incubated for another 2 h at 37 °C. The absorbance was measured with a microplate reader at 450 nm. Viability of treated cell wells was expressed as a percentage of the viability of control wells without treatment.

Conclusions

We have developed novel pRF-GQDs with a sharp fluorescence transition at pH 6.8 and demonstrated that pRF-GQDs enable detecting solid tumors of different origin at an early stage. Due to the unique two-phase fluorescence switch between tumors and healthy tissues, their excellent safety profile, and their high specificity and sensitivity to tumors, pRF-GQDs have great potential to be used as a universal probe in clinic for fluorescence-guided cancer surgery or cancer diagnosis. In addition, electrochemical reaction, as an effective approach to dope carbon materials with heteroatoms, makes it possible to fine alter their intrinsic properties and produces new characteristics. It is likely that further tuning the atoms doping approach described in this study allow synthesis of GQDs responding to pHs other than 6.8.

Supplementary Material

Refer to Web version on PubMed Central for supplementary material.

Acknowledgments

This work was supported by NSFC grant 21573019 (LF), NSFC Major Research Plan grant 21233003 (LF), Central Universities Fundamental Research Funds (LF), and NIH grant NS095817 (JZ). The authors would also like to sincerely thank Prof. Mengchao Cui and Mr. Kaixiang Zhou (Department of Chemistry, Beijing Normal University) for assistance with *in vivo* imaging.

Notes and references

1. Hirsch FR, Franklin WA, Gazdar AF, Bunn PA. Clin Cancer Res. 2001; 7:5–22. [PubMed: 11205917]
2. Nothacker M, Duda V, Warm M, Degenhardt F, Madjar H, Weinbrenner S, Albert US. BMC Cancer. 2009; 9:1–9. [PubMed: 19118499]
3. Nguyen QT, Tsien RY. Nat Rev Cancer. 2013; 13:653–662. [PubMed: 23924645]
4. Shariat SF, Karakiewicz PI, Ashfaq R, Lerner SP, Palapattu GS, Cote RJ, Sagalowsky AI, Lotan Y. Cancer. 2008; 112:315–325. [PubMed: 18008359]
5. Cheang MCU, Voduc D, Bajdik C, Leung S, McKinney S, Chia SK, Perou CM, Nielsen TO. Clin Cancer Res. 2008; 14:1368–1376. [PubMed: 18316557]
6. Arya SK, Bhansali S. Chem Rev. 2011; 111:6783–6809. [PubMed: 21774490]
7. Stephan C, Cammann H, Meyer HA, Lein M, Jung K. Cancer Lett. 2007; 249:18–29. [PubMed: 17292541]
8. Shukla HD, Mahmood J, Vujaskovic Z. Cancer Lett. 2015; 369:28–36. [PubMed: 26276717]
9. Kim JW, Dang CV. Cancer Res. 2006; 66:8927–8930. [PubMed: 16982728]
10. Brahimi-Horn MC, Pouyssegur J. Febs Lett. 2007; 581:3582–3591. [PubMed: 17586500]
11. Vaupel P, Kallinowski F, Okunieff P. Cancer Res. 1989; 49:6449–6465. [PubMed: 2684393]
12. Helmlinger G, Yuan F, Dellian M, Jain RK. Nat Med. 1997; 3:177–182. [PubMed: 9018236]
13. Volk T, Jahde E, Fortmeyer HP, Glusenkamp KH, Rajewsky MF. Br J Cancer. 1993; 68:492–500. [PubMed: 8353039]
14. Wang Y, Zhou K, Huang G, Hensley C, Huang X, Ma X, Zhao T, Sumer BD, DeBerardinis RJ, Gao J. Nat Mater. 2014; 13:204–212. [PubMed: 24317187]
15. Urano Y, Asanuma D, Hama Y, Koyama Y, Barrett T, Kamiya M, Nagano T, Watanabe T, Hasegawa A, Choyke PL, Kobayashi H. Nat Med. 2009; 15:104–109. [PubMed: 19029979]
16. Li C, Xia JA, Wei XB, Yan HH, Si Z, Ju SH. Adv Funct Mater. 2010; 20:2222–2230.
17. Pan D, Zhang J, Li Z, Wu M. Adv Mater. 2010; 22:734–738. [PubMed: 20217780]
18. Li L, Ji J, Fei R, Wang C, Lu Q, Zhang J, Jiang L, Zhu J. Adv Funct Mater. 2012; 22:2971–2979.
19. Liu R, Wu D, Feng X, Muellen K. J Am Chem Soc. 2011; 133:15221–15223. [PubMed: 21894989]
20. Eda G, Lin Y, Mattevi C, Yamaguchi H, Chen H, Chen I, Chen C, Chhowalla M. Adv Mater. 2010; 22:505–509. [PubMed: 20217743]
21. Shen J, Zhu Y, Yang X, Li C. Chem Commun. 2012; 48:3686–3699.
22. Li Y, Zhao Y, Cheng H, Hu Y, Shi G, Dai L, Qu L. J Am Chem Soc. 2012; 134:15–18. [PubMed: 22136359]
23. Yuan F, Li S, Fan Z, Meng X, Fan L, Yang S. Nano Today. 2016; 11:565–586.
24. Fan Z, Li S, Yuan F, Fan L. RSC Adv. 2015; 5:19773–19789.
25. Jia X, Li J, Wang E. Nanoscale. 2012; 4:5572–5575. [PubMed: 22786671]
26. Li S, Li Y, Cao J, Zhu J, Fan L, Li X. Anal Chem. 2014; 86:10201–10207. [PubMed: 25280346]
27. Xie W, Fu Y, Ma H, Zhang M, Fan L. Acta Chim Sin. 2012; 70:2169–2172.
28. Wang Y, Meng Y, Wang S, Li C, Shi W, Chen J, Wang J, Hong R. Small. 2015; 29:3575–3581.

29. Fan Z, Li Y, Li X, Fan L, Zhou S, Fang D, Yang S. Carbon. 2014; 70:149–156.
30. Tan X, Li Y, Li X, Zhou S, Fan L, Yang S. Chem Commun. 2015; 51:2544–2566.
31. Guo R, Zhou S, Li Y, Li X, Fan L, Nicolas HV. ACS Appl Mater Interfaces. 2015; 7:23958–23966. [PubMed: 26317667]
32. Zhu S, Zhang J, Qiao C, Tang S, Li Y, Yuan W, Li B, Tian L, Liu F, Hu R, Gao H, Wei H, Zhang H, Sun H, Yang B. Chem Commun. 2011; 47:6858–6860.
33. Wu Z, Gao M, Wang T, Wan X, Zheng L, Huang C. Nanoscale. 2014; 6:3868–3874. [PubMed: 24589665]
34. Zhang M, Bai L, Shang W, Xie W, Ma H, Fu Y, Fang D, Sun H, Fan L, Han M, Liu C, Yang S. J Mater Chem. 2012; 22:7461–7467.
35. Shang W, Zhang X, Zhang M, Fan Z, Sun Y, Han M, Fan L. Nanoscale. 2014; 6:5799–5806. [PubMed: 24740121]
36. Yuan F, Ding L, Li Y, Li X, Fan L, Zhou S, Fang D, Yang S. Nanoscale. 2015; 7:11727–11733. [PubMed: 26102292]
37. Pan D, Zhang J, Li Z, Wu C, Yan X, Wu M. Chem Commun. 2010; 46:3681–3683.
38. Jain RK. Cancer Metast Rev. 1987; 6:559–593.

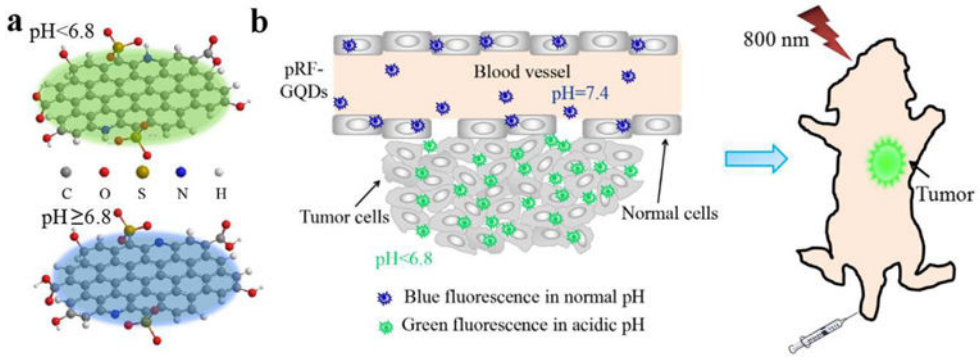

Fig. 1.

Schematic diagrams of pRF-GQDs under different pHs (a) and their application for tumor imaging (b).

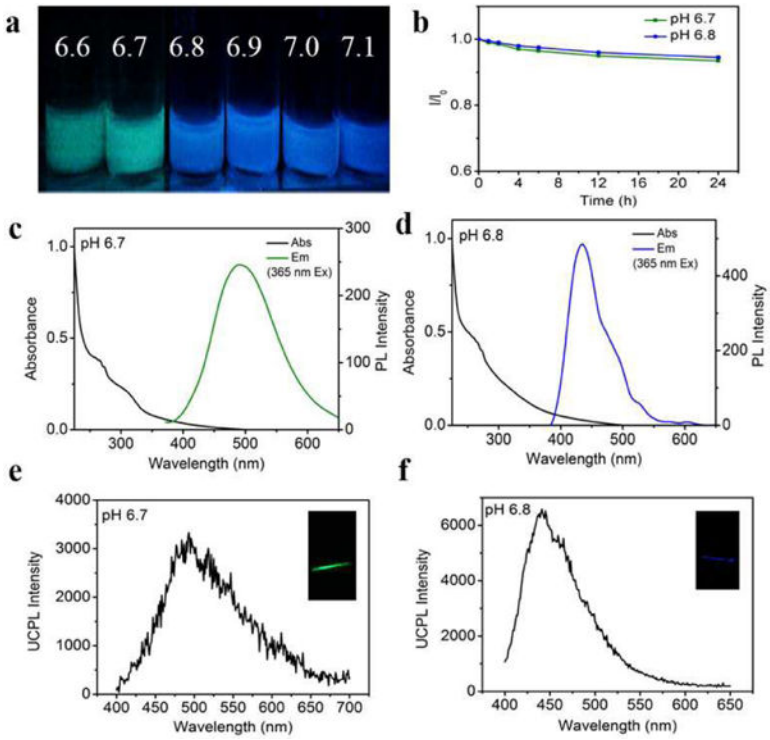

Fig. 2.

Characterization of the photoluminescence property and UCPL property of pRF-GQDs. (a) Representative images of pRF-GQDs under indicated pHs. (b) Photostabilities of pRF-GQDs. pRF-GQDs in solution were continuously irradiated using a 400 W xenon lamp. I and I_0 represent the fluorescence intensities at the emission peak before and after irradiation, respectively. After 24 h irradiation, no obvious decrease was seen. (c, d) UV-*vis* absorption and photoluminescence spectra of pRF-GQDs at pH 6.7 (c) and pH 6.8 (d). (e, f) UCPL spectra and photographs (insets) of pRF-GQDs at pH 6.7 (e) and pH 6.8 (f).

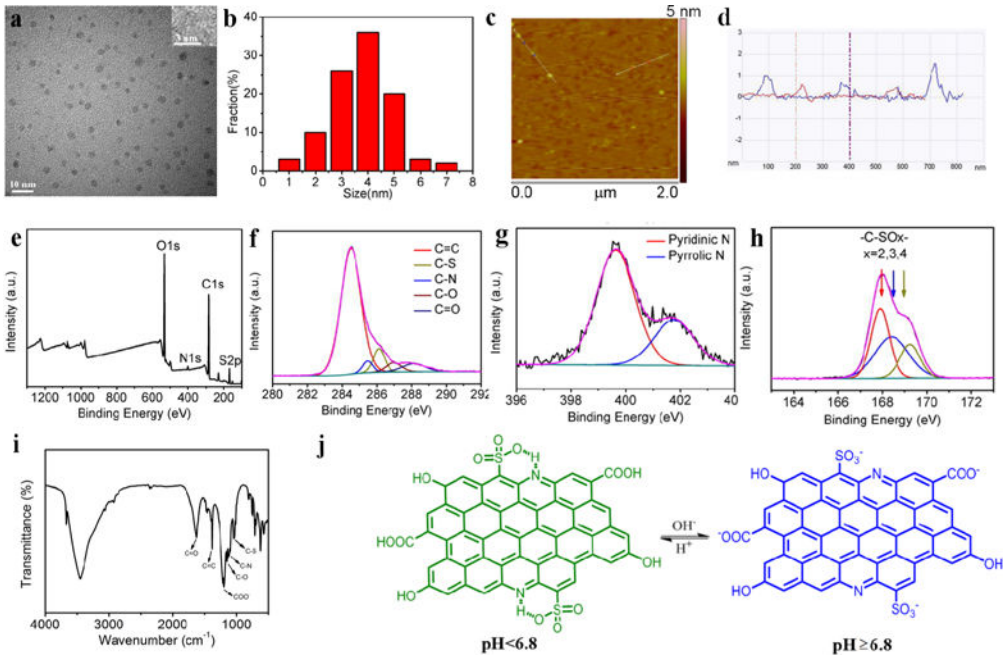

Fig. 3.

Characterization of the physical and chemical properties of pRF-GQDs. (a) TEM, HRTEM (inset) images of pRF-GQDs. (b) Size distribution of pRF-GQDs. (c) AFM image of pRF-GQDs. (d) Height profile of pRF-GQDs deposited on freshly cleaved mica substrates. (e–h) XPS analysis of pRF-GQDs. (i) IR spectra of pRF-GQDs. (j) Proposed mechanism accounting for the pH response property of pRF-GQDs.

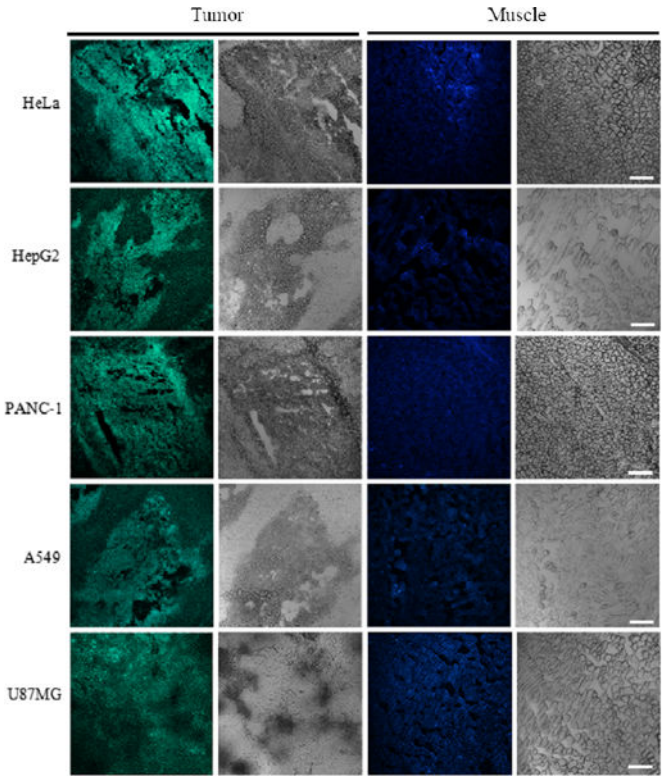

Fig. 4.

pRF-GQDs for in situ detection of tumors. Representative confocal microscopy images of indicated tumors under green fluorescence channel and white field (left two panels) and adjacent muscles under blue fluorescence channel and white field (right two panels). Scale bar: 40 μm.

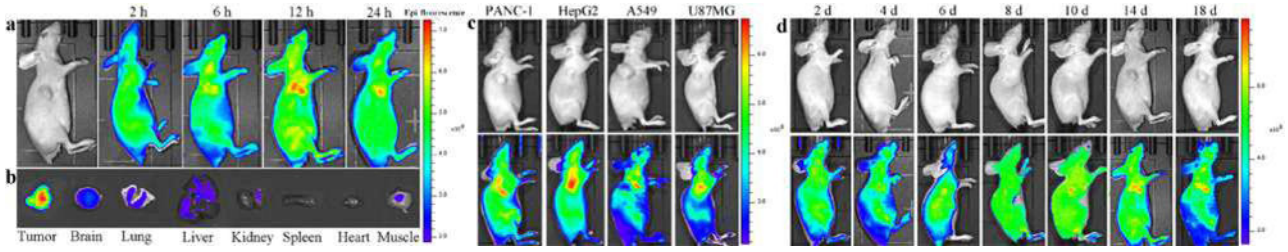

Fig. 5.

pRF-GQDs for non-invasive detection of tumors in live animals. (a) Representative images of a HeLa tumor-bearing mouse at the indicated time points after intravenous injection of pRF-GQDs (10 mg/kg). (b) *Ex vivo* imaging of major organs from a mouse treated with pRF-GQDs. The mouse was sacrificed 24 hours after injection. (c) Representative images of mice bearing the indicated tumors at 12 hours after intravenous injection of pRF-GQDs (10 mg/kg). (d) Representative images of a HeLa tumor-bearing mouse at the indicated time points after tumor inoculation. The average intensities of fluorescence in the tumor sites were 2.8, 3.2, 6.8, 7.3, 7.9, 8.2, 8.5 ($\times 10^8$ p/sec/cm^2/sr) on day 2, 4, 6, 8, 10, 14, 18 post inoculation. Mice were intravenously administrated with pRF-GQDs solution at a dose of 5 mg/kg every two days. Twelve hours after each injection, mice were imaged.

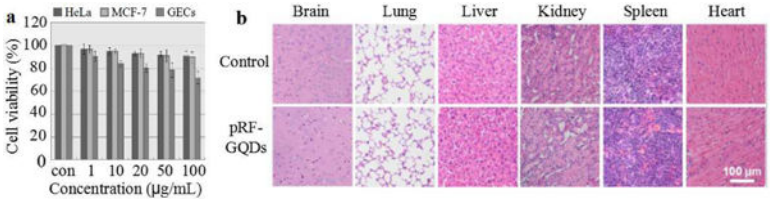

Fig. 6.

Toxicity of pRF-GQDs. (a) Cytotoxicity of pRF-GQDs on indicated cells. (b) Representative images of indicated tissues with H&E staining.